ISSN 0023-1584, Kinetics and Catalysis, 2011, Vol. 52, No. 1, pp. 139–144. © Pleiades Publishing, Ltd., 2011.
Original Russian Text © D.I. Potemkin, P.V. Snytnikov, V.D. Belyaev, V.A. Sobyanin, 2011, published in Kinetika i Kataliz, 2011, Vol. 52, No. 1, pp. 143–148.

VIII INTERNATIONAL CONFERENCE
ON MECHANISMS OF CATALYTIC REACTIONS

Effect of Internal Diffusion on Preferential CO Oxidation in a Hydrogen-Rich Mixture on a Copper–Cerium Oxide Catalyst in a Microchannel Reactor

D. I. Potemkin[a,b], P. V. Snytnikov[a,b], V. D. Belyaev[a,b], and V. A. Sobyanin[a,b]

[a] *Boreskov Institute of Catalysis, Siberian Branch, Russian Academy of Sciences, Novosibirsk, 630090 Russia*

[b] *Novosibirsk State University, Novosibirsk, 630090 Russia*

e-mail: pvsnyt@catalysis.ru

Received September 30, 2009

Abstract—The effect of internal diffusion on preferential CO oxidation in a hydrogen-rich mixture on a copper–cerium catalyst in a microchannel reactor was estimated. It was found that the internal effectiveness factor $\eta_{CO} > 0.8$ was reached at a catalytic coating thickness of ~30 μm.

DOI: 10.1134/S0023158410061011

INTRODUCTION

Increasing the efficiency of the deep purification of hydrogen-rich mixtures to remove carbon monoxide has long been considered an important problem. Interest in this problem has quickened in the past few years because of the use of hydrogen-rich mixtures for feeding proton-exchange membrane fuel cells (PEMFCs). Hydrogen-rich mixtures prepared from hydrocarbon materials with the subsequent steam conversion of CO usually contain 0.5–2 vol % CO. Because CO is a poison for the PEMFC anode, its concentration should be decreased to a level of <10 ppm.

A promising method for the removal of CO from a hydrogen-rich mixture is the selective oxidation of carbon monoxide including the following two main reactions:

$$2CO + O_2 = 2CO_2; \quad (1)$$

$$2H_2 + O_2 = 2H_2O. \quad (2)$$

Reaction (II) of hydrogen oxidation results in a loss of fuel for PEMFCs and decreases the process efficiency; therefore, it is desirable to minimize the contribution of this reaction.

Au, Pt, Ru, Rh, Co, and Cu catalysts on various supports are active in the reaction of preferential CO oxidation [1–26]. Copper–cerium oxide systems are considered sufficiently active, most selective [7–24], and less expensive, as compared with catalysts based on platinum-group metals and gold. This allowed us to consider them as very promising catalysts for practical applications.

In the development of miniature fuel processors for portable PEMFCs, it is most reasonable to use a microchannel reactor for the selective oxidation of CO [27]. The advantages of the use of these reactors for performing the highly exothermic reaction of preferential CO oxidation over traditional catalytic fixed-bed reactors have been demonstrated in a number of publications [23–26, 28]. The catalyst bed is supported onto the walls of microchannels as a thin coating. This makes it possible to perform efficient heat and mass transfer and to operate under nearly isothermal conditions to prevent the occurrence of side reactions (the oxidation of hydrogen, the reverse water gas shift reaction, and the methanization of carbon oxides) and to provide the required degree of CO removal over a wide temperature range [24–26].

The use of thin-layer catalytic coatings also makes it possible to minimize internal-diffusion limitation. According to published data [26], the effect of internal diffusion on the selective oxidation of CO in a microchannel reactor with a $Pt/\gamma\text{-}Al_2O_3$ catalyst at a coating thickness of 2–5 μm is insignificant. On the other hand, even on small $Pt/\gamma\text{-}Al_2O_3$ pellets 360 μm in diameter, the internal effectiveness factor decreased to 0.5 at a temperature of 250°C [4]. Evidently, the use of pellets with a radius of approximately 5 μm in a fixed-bed reactor is very difficult because of high pressure drop, whereas the use of a skin catalyst inevitably increases the reactor volume.

Snytnikov et al. [24] used the Thiele–Zeldovich modulus to evaluate the effect of internal diffusion on the course of the preferential CO oxidation on a copper–cerium oxide catalyst. At a pellet radius of ~100 μm, the effect of internal diffusion can manifest itself even at temperatures of about 200°C. To perform more accurate calculations, data on the texture characteristics of the catalyst and the kinetics of occurring reactions are required.

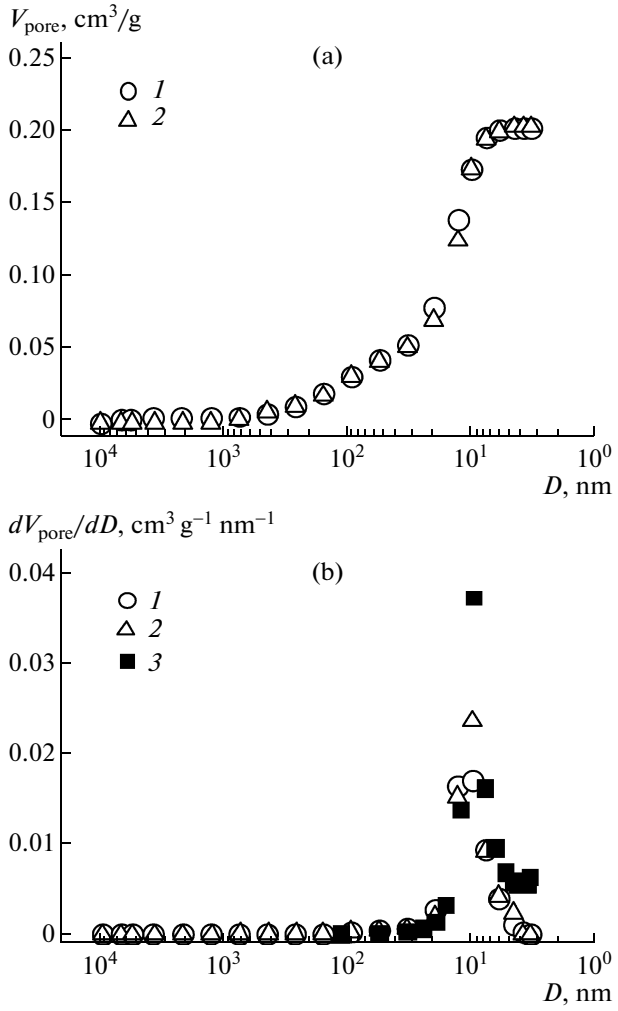

Fig. 1. (a) Dependence of the volume of impressed mercury on pore size for (*1*) CuCe(I) and (*2*) CuCe(R) catalysts. (b) Pore size distribution in (*1*) CuCe(I) and (*2*) CuCe(R) catalysts, as measured by mercury porosimetry, and (*3*) the CuCe(R) sample, as found by an analysis of the desorption branch of a full isotherm of low-temperature nitrogen adsorption.

In this work, we used data on the pore structure of a copper–cerium oxide catalyst and the kinetics of reactions to evaluate the effect of internal diffusion on the reaction of preferential CO oxidation in a microchannel reactor for optimizing the thickness of catalytic coatings supported onto the walls of microchannels.

EXPERIMENTAL

Synthesis of Catalysts and Preparation of Catalytic Coatings

The direct examination of the pore structure of coatings using currently available standard procedures is difficult to perform. Therefore, in this work, we synthesized a (5 wt % Cu)/CeO_2 powdered catalyst based on previously described procedures for the preparation of catalytic coatings on the walls of microchannels formed in stainless steel plates with the use of an aqueous suspension of cerium oxide and polyvinyl alcohol [23, 24]. The suspension was calcined at 400°C for 2 h to obtain cerium oxide powder, which was incipient wetness impregnated with an aqueous solution of $Cu(NO_3)_2$, dried in air at room temperature, and calcined at 400°C for 2 h. Henceforth, the catalyst thus prepared is referred to as CuCe(I).

To evaluate changes in the CuCe(I) catalyst under reaction conditions, it was treated at 220°C for 4 h with a mixture consisting of CO, O_2, H_2O, CO_2, and H_2, whose partial pressures were 1.0, 1.5, 10, 20, and 65 kPa, respectively, with the balance He (to atmospheric pressure). The supply rate of the mixture (at standard temperature and pressure) on a catalyst weight basis was 14400 cm^3 g^{-1} h^{-1}. Henceforth, this catalyst sample is referred to as CuCe(R).

Investigation Techniques

The specific surface areas (S_{BET}) of catalysts, pore volumes, and pore size distributions were measured by analyzing full isotherms of low-temperature nitrogen adsorption at −196°C obtained on an ASAP-2400 instrument.

The pore volume and pore size distribution was also determined by mercury porosimetry on an AutoPore IV 9500 instrument. The texture characteristics were calculated using a model of uncrossing cylindrical pores. Catalyst powders were pressed into pellets before the measurement.

The high-resolution transmission electron microscopic (HR TEM) images of the samples were obtained on a JEM-2010 instrument (lattice resolving power of 0.14 nm at an accelerating voltage of 200 kV). The images of periodic structures were analyzed by the Fourier method.

RESULTS AND DISCUSSION

Texture Characteristics of Catalysts

Figure 1 shows the dependence of the volume of impressed mercury on pore diameter and pore size distributions in CuCe(I) and CuCe(R) samples. Both of these plots are similar; this fact suggests the absence of considerable catalyst texture changes under the action of a reaction mixture. At the pore diameter D = 500 nm or higher, the volume of impressed mercury remained almost unchanged; this fact suggests the absence of so large pores in the samples. The volume of impressed mercury increased as the pore diameter was decreased starting with 500 nm.

The pore size distribution in the mesopore region found using mercury porosimetry is consistent with data obtained by the analysis of a desorption branch of the full isotherm of low-temperature nitrogen adsorp-

tion (Figure 1b shows the distribution only for the CuCe(R) catalyst; the distribution for CuCe(I) was analogous). The total pore volume in both of the catalysts was 0.2 cm^3/g, which is consistent with data obtained by the low-temperature adsorption of nitrogen (Table 1).

As can be seen in Fig. 1b, pores with diameters smaller than 20 nm made the main contribution to the pore space volume of the CuCe(I) and CuCe(R) catalysts; a maximum was observed in the region of ~10 nm. Larger pores 20 to 500 nm in diameter also made an appreciable contribution (about a third of the total pore volume) (Fig. 1a). According to distribution data, the average pore size (d_{pore}) was 46 nm. Other texture characteristics of the catalysts, namely, porosity (ε) and tortuosity (τ), were also estimated using mercury porosimetry; the found values were 0.6 and 2, respectively (Table 1).

In general, the observed dependences were qualitatively consistent with electron-microscopic data. As an example, Fig. 2 shows the micrographs of the CuCe(I) catalyst. The micrographs of the CuCe(R) catalyst were analogous, and they are not given here. Because copper in a disperse state is extremely difficult to distinguish from cerium because Cu is lighter than Ce [21], the resulting images are homogeneous. Cerium oxide consists of crystallites of size 5–10 nm (Fig. 2a), which combined to form large porous agglomerates whose size is hundreds of nanometers (Fig. 2b).

Because the procedure used to prepare a catalytic coating in microreactor channels was analogous to that used to prepare the CuCe(I) catalyst as powder, whose texture characteristics did not change under the action of a reaction atmosphere, we believed that the pore size of the catalytic coating and the pore size distribution should be approximately the same as those in the CuCe(I) and CuCe(R) samples.

Effect of Internal Diffusion

According to published data [15, 18–24, 29, 30], reactions (I) and (II) under conditions of the selective oxidation of CO on a copper–cerium oxide catalyst can be considered as two independent processes in which a common reactant (oxygen) is consumed. Previously [29, 30], the reaction kinetics of H_2 and CO oxidation under conditions of the selective oxidation of CO on a 5 wt % Cu/CeO_2 catalyst in a microchannel reactor was studied over the temperature range of 130–170°C at low degrees of reactant conversion (x_{CO} and x_{O_2} of <10%) and a catalytic coating thickness of 40 μm. Under these conditions, as estimated using well-known criteria (Thiele–Zeldovich and Weisz–Prater criteria), the reaction occurred in the kinetic region.

To approximately describe the observed kinetic dependences, we used power-law rate expressions with rate constants in Arrhenius form:

Table 1. Texture characteristics of the catalysts

Characteristic	CuCe(I)	CuCe(R)
Specific surface area S_{BET}, m^2/g	80	77
Pore volume V_{pore}, cm^3/g	0.2 (0.21*)	0.2 (0.21*)
Average pore diameter d_{pore}, nm	46	46
Porosity ε	0.6	0.6
Tortuosity τ	2	2

* Obtained by an analysis of low-temperature nitrogen adsorption isotherms.

$$w_{CO} = -k_{CO}P_{CO}^{a}P_{O_2}^{b} \text{ mol } m_{Cat}^{-3}\ s^{-1},$$
$$\text{where } k_{CO} = 5.3 \times 10^{11}\exp\left(-\frac{E_a^{CO}}{RT}\right), \quad (3)$$

$$w_{H_2} = -k_{H_2}P_{O_2}^{n} \text{ mol } m_{Cat}^{-3}\ s^{-1},$$
$$\text{where } k_{H_2} = 8.2 \times 10^{17}\exp\left(-\frac{E_a^{H_2}}{RT}\right). \quad (4)$$

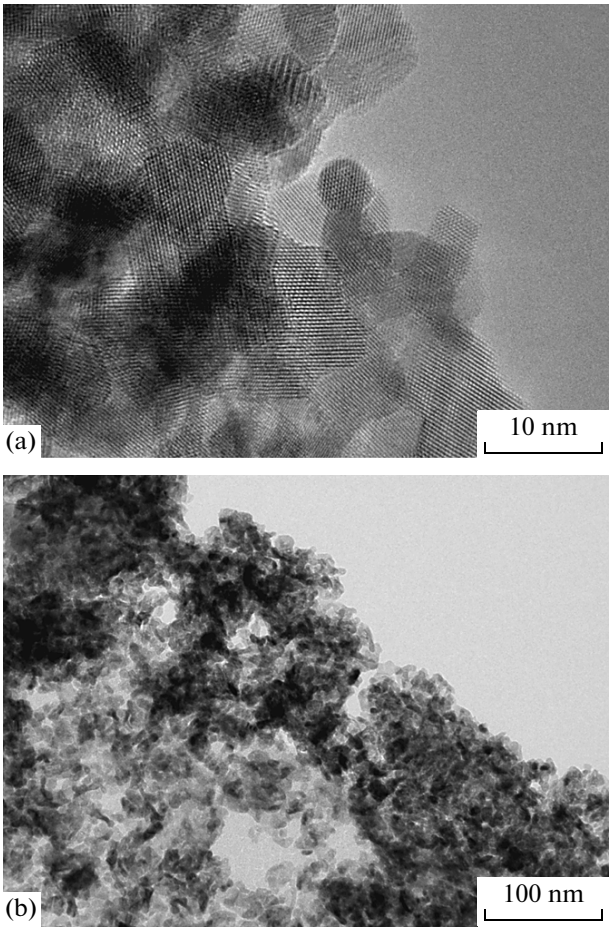

Fig. 2. Micrographs of the CuCe(I) catalyst.

Table 2. Kinetic parameters of CO and H_2 oxidation on copper–cerium oxide catalysts

Partial pressure, kPa					Kinetic parameters					
					CO oxidation			H_2 oxidation		references
CO	O_2	CO_2	H_2O	H_2	a	b	E_a, kJ/mol	n	E_a, kJ/mol	
0.14–5.2	0.5–3.1	25	10	50	0.9	0	86	0	151	29, 30
0.5–4.0	0.5–4.0	4–16	4–20	10–50	0.91	0	94	0	142	19

The units of measurement of the partial pressures P_{CO} and P_{O_2} are kilopascals. In the expression for the reaction rate of hydrogen oxidation, a change in the concentration of H_2 can be ignored because hydrogen was present in large excess and its concentration remained almost unchanged in the course of reaction. The apparent activation energies of CO and H_2 oxidation, as well as the orders of reaction with respect to CO and O_2, are summarized in Table 2. As can be seen in Table 2, the found kinetic parameters [29, 30] are close to those obtained by another research group [19] under conditions of the selective oxidation of CO. These parameters allowed us to describe catalytic functions observed in a fixed-bed flow reactor in the integral mode with a good accuracy.

For preferential CO oxidation under steady-state conditions in the absence of temperature gradients in the catalyst bed uniformly supported onto the inner surface of a cylindrical channel, CO and O_2 material balance equations with the internal mass transport limitations taken into account can be written in the following form:

$$\frac{D_{CO}^{eff}}{RT}\left(\frac{d}{dr}\left(\frac{dP_{CO}}{dr}\right)+\frac{1}{r}\frac{dP_{CO}}{dr}\right)-k_{CO}P_{CO}^{a}P_{O_2}^{b}=0, \quad (5)$$

$$\frac{D_{O_2}^{eff}}{RT}\left(\frac{d}{dr}\left(\frac{dP_{O_2}}{dr}\right)+\frac{1}{r}\frac{dP_{O_2}}{dr}\right)-\frac{1}{2}\left(k_{CO}P_{CO}^{a}P_{O_2}^{b}+k_{H_2}P_{O_2}^{n}\right)=0, \quad (6)$$

where D_{CO}^{eff} and $D_{O_2}^{eff}$ are the effective diffusion coefficients of CO and O_2 in m^2/s, respectively; $r = R_1$ is the radius of the part of the microchannel free of catalyst; and $r = R_2$ is the radius of the initial microchannel without a catalytic coating. Boundary conditions for Eqs. (3) and (4): the partial pressures of reactants at the surface of the catalytic coating correspond to pressures in a gas phase, that is, $P_{CO} = P_{CO(gas)}$ and $P_{O_2} = P_{O_2(gas)}$; the first derivatives of the partial pressures of reactants at the microchannel walls are $\frac{dP_{CO}}{dr} = 0$ and $\frac{dP_{O_2}}{dr} = 0$. In the microchannel reactors used previously [23, 24], $R_2 = 250$ μm and $R_1 = 210$–230 μm because the coating thickness ($h = R_2 - R_1$) varied over a range of 20–40 μm depending on the amount of supported catalyst. In our calculations, we fixed the dimension R_2 on varying the coating thickness h from 0 to 100 μm.

To solve the set of Eqs. (3) and (4), it is necessary to know the effective diffusion coefficients of CO and O_2. Because the pore size distribution was found sufficiently broad and the free paths of CO and O_2 molecules under these conditions (which varied over the range of 50–60 nm depending on temperature) were close to the average pore diameter (46 nm), it is difficult to unambiguously determine which type of diffusion was predominant: molecular diffusion or diffusion according to the Knudsen mechanism. It is most likely that the reaction occurred in the transition region. Therefore, we considered two extreme variants: when substance transfer in catalyst pores occurs by the mechanism of molecular diffusion and by the Knudsen mechanism.

In the former case, the effective diffusion coefficient D_i^{eff} is proportional to the molecular diffusion coefficient D_i^{mol}, and the calculation was performed using the equation

$$D_i^{eff} = D_i^{mol}\frac{\varepsilon}{\tau} = \frac{1}{3}\lambda_i U_i \frac{\varepsilon}{\tau}, \quad (7)$$

where λ_i is the free path of diffusing substance molecules in the reaction mixture; $U_i = \sqrt{8RT/\pi M_i}$ is the average thermal velocity of the molecules of ith diffusing substance with the molecular weight M_i, ε is the porosity, and τ is the pore tortuosity. The molecular free path was calculated from the formula $\lambda_i \approx U_i/\sum_j \sigma_{ij}\overline{U}_{ij}n_j$, where σ_{ij} is the gas-kinetic collision cross section of molecules i and j (reference values [32] were used); $\overline{U}_{ij} = \sqrt{8RT(M_i + M_j)/\pi M_i M_j}$ is the average relative thermal velocity of molecules i and j; and n_j is the concentration of molecules of substance j. Pair coefficients of all of the substances present in the model mixture (CO, O_2, H_2, CO_2, H_2O, and He) were taken into account in the calculations.

In the latter case, the effective diffusion coefficient D_i^{eff} is proportional to the Knudsen diffusion coefficient (D_i^{Kn}) [31, 33], and the calculation was performed using the equation

$$D_i^{eff} = D_i^{Kn}\frac{\varepsilon}{\tau} = \frac{1}{3}d_{pore}\sqrt{\frac{8RT}{\pi M_i}}\frac{\varepsilon}{\tau}, \quad (8)$$

where d_{pore} is the average catalyst pore diameter calculated based on the full pore size distribution.

The effect of internal diffusion on the course of the selective oxidation of CO was characterized by the internal effectiveness factor (η_{CO}), which was determined as the ratio of the reaction rate in the presence of diffusion limitation to the rate in the absence of this limitation:

$$\eta_{CO} = \frac{2\pi \int_{R_1}^{R_2} w_{CO}(r) r dr}{\pi h (R_2 + R_1) w_{CO}}. \quad (9)$$

Note that, because the reaction of hydrogen oxidation is of zero order with respect to oxygen (Table 2) and hydrogen occurs in a considerable excess, as compared with other reactants, $\eta_{H_2} \approx 1$ under conditions of preferential CO oxidation.

The numerical solution of Eqs. (3), (4), and (9) was performed by the Radau 5 method using the Mathcad 14 software package in all cases. The calculations were performed as applied to the following conditions: temperature range of 150–230°C; atmospheric pressure; and a hydrogen-rich mixture composition typical of preferential CO oxidation, in which the partial pressures of CO, O_2, H_2O, CO_2, and H_2 were 1.0, 1.5, 10, 20, and 65 kPa, respectively, with the balance He (to atmospheric pressure).

Figures 3a and 3b show the dependence of η_{CO} on catalytic coating thickness h and reaction temperature in the course of diffusion by the molecular mechanism and the Knudsen mechanism, respectively. It can be seen that an increase in the coating thickness or temperature resulted in a decrease in η_{CO}. At a coating thickness of 40 μm, the value of η_{CO} was higher than 0.95 in any diffusion mechanism up to a temperature of 190°C. An increase in the temperature to 230°C was accompanied by a decrease in η_{CO} to 0.79 and 0.69 under conditions of molecular and Knudsen diffusion, respectively. At a coating thickness of 20 μm, the internal effectiveness factor was higher than 0.9 at 230°C. Because the value of η_{CO} in the reaction of H_2 oxidation under the given conditions was close to 1 and independent of catalytic coating thickness, an increase in the amount of supported catalyst will additionally facilitate a decrease in the process selectivity with temperature. Previously [23, 24], we found that an optimum reaction temperature for the selective oxidation of CO on a copper–cerium oxide catalyst in a microchannel reactor varied from 170 to 230°C depending on contact time. Taking into account these results, we can conclude that the catalytic coating thickness should be no greater than 30 μm; in this case, the inner surface efficiency factor will be higher than 0.8 regardless of diffusion mechanism.

Currently, it is generally recognized that highly dispersed copper on the surface of cerium oxide is the active component of copper–cerium oxide catalysts

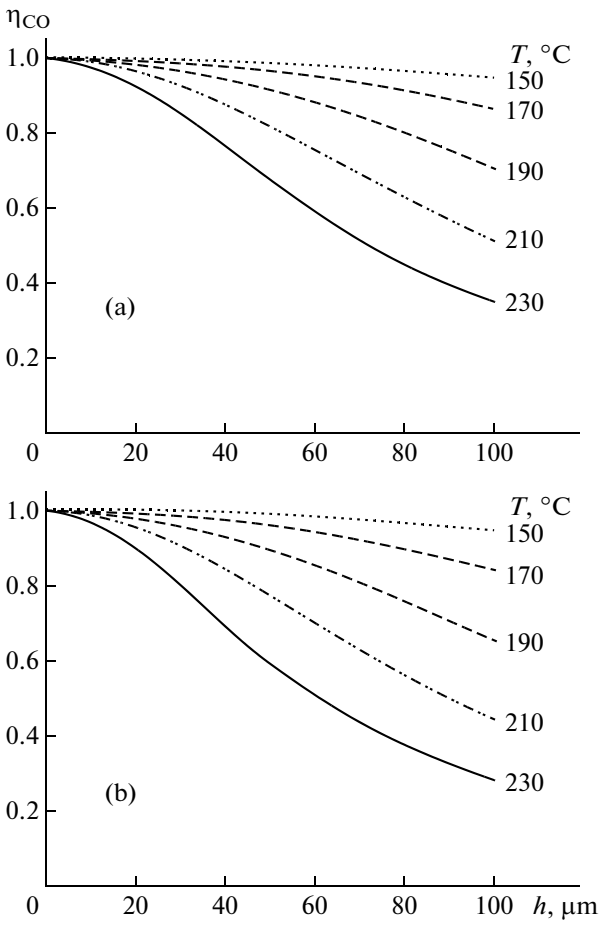

Fig. 3. Dependence of the efficiency factor η_{CO} at the microchannel reactor inlet on coating thickness h and temperature for diffusion by (a) molecular and (b) Knudsen mechanisms.

for the selective oxidation of CO [9–24]. In this context, many researchers [9–13, 22] attempted to improve a procedure for preparing copper–cerium catalysts in order to increase their activity and selectivity by increasing specific surface area. As a rule, this was reached by decreasing the size of CeO_2 crystallites; in turn, this decreased the average pore diameter in the catalyst. Catalyst pellets of size from 100 to 500 μm are commonly used in catalytic experiments; therefore, it is reasonable to believe that, under these conditions, the reaction of preferential CO oxidation occurred in the region of internal-diffusion limitation. This adequately explains why the observed catalytic characteristics of samples prepared by various methods were often similar and weakly dependent on the specific surface area of the catalyst. In our opinion, it is most reasonable to obtain a copper–cerium oxide catalyst whose texture characteristics provide effective mass transfer in pores.

ACKNOWLEDGMENTS

We are grateful to M.S. Mel'gunov, V.B. Fenelonov, A.V. Ishchenko, and S.I. Reshetnikov for their assistance in performing a number of experiments and constructive discussions of the experimental results.

This study was supported in part through the Program "UMNIK" of the Science and Technology Small Business Support Foundation and through the Federal Targeted Program "Research and Pedagogical Cadres of Innovative Russia" (state contract no. P185 of July 16, 2009, for the years 2009–2013).

REFERENCES

1. Manasilp, A. and Gulari, E., *Appl. Catal., B*, 2002, vol. 37, p. 17.
2. Schubert, M.M., Gasteiger, H.A., and Behm, R.J., *J. Catal.*, 1997, vol. 172, p. 256.
3. Kahlich, M.J., Gasteiger, H.A., and Behm, R.J., *J. Catal.*, 1997, vol. 171, p. 93.
4. Kim, D.H. and Lim, M.S., *Appl. Catal., A*, 2002, vol. 224, p. 27.
5. Denkwitz, Y., Schumacher, B., Kucerova, G., and Behm, R.J., *J. Catal.*, 2009, vol. 267, p. 78.
6. Galletti, C., Fiorot, S., Specchia, S., Saracco, G., and Specchia, V., *Chem. Eng. J.*, 2007, vol. 134, p. 45.
7. Avgouropoulos, G., Ioannides, T., Matralis, H.K., Batista, J., and Hocevar, S., *Catal. Lett.*, 2001, vol. 73, p. 33.
8. Martınez-Arias, A., Hungrıa, A.B., Munuera, G., and Gamarra, D., *Appl. Catal., B*, 2006, vol. 65, p. 207.
9. Avgouropoulos, G. and Ioannides, T., *Appl. Catal., A*, 2003, vol. 244, p. 155.
10. Avgouropoulos, G. and Ioannides, T., *Appl. Catal., B*, 2006, vol. 67, p. 1.
11. Liu, Z., Zhou, R., and Zheng, X., *J. Mol. Catal. A: Chem.*, 2007, vol. 267, p. 137.
12. Luo, M.-F., Ma, J.-M., Lu, J.-Q., Song, Y.-P., and Wang, Y.-J., *J. Catal.*, 2007, vol. 246, p. 52.
13. Zhang, Y., Liang, H., Gao, X.Y., and Liu, Y., *Catal. Commun.*, 2009, vol. 10, p. 1432.
14. Martinez-Arias, A., Fernandez-Garcia, M., Galvez, O., Coronado, J.M., Anderson, J.A., Conesa, J.C., Soria, J., and Munuera, G., *J. Catal.*, 2000, vol. 195, p. 207.
15. Sedmak, G., Hocevar, S., and Levec, J., *J. Catal.*, 2003, vol. 213, p. 135.
16. Sedmak, G., Hocevar, S., and Levec, J., *J. Catal.*, 2004, vol. 222, p. 87.
17. Sedmak, G., Hocevar, S., and Levec, J., *Top. Catal.*, 2004, vols. 30–31, p. 445.
18. Moreno, M., Baronetti, G.T., Laborde, M.A., and Marino, F.J., *Int. J. Hydrogen Energy*, 2008, vol. 33, p. 3538.
19. Lee, H.C. and Kim, D.H., *Catal. Today*, 2008, vol. 132, p. 109.
20. Snytnikov, P.V., Stadnichenko, A.I., Semin, G.L., Belyaev, V.D., Boronin, A.I., and Sobyanin, V.A., *Kinet. Katal.*, 2007, vol. 48, p. 463 [*Kinet. Catal.* (Engl. Transl.), vol. 48, p. 439].
21. Snytnikov, P.V., Stadnichenko, A.I., Semin, G.L., Belyaev, V.D., Boronin, A.I., and Sobyanin, V.A., *Kinet. Katal.*, 2007, vol. 48, p. 472 [*Kinet. Catal.* (Engl. Transl.), vol. 48, p. 448].
22. Potemkin, D.I., Snytnikov, P.V., Pakharukova, V.P., Semin, G.L., Moroz, E.M., and Sobyanin, V.A., *Kinet. Katal.*, 2010, vol. 51, no. 1, p. 129 [*Kinet. Catal.* (Engl. Transl.), vol. 51, no. 1, p. 119].
23. Snytnikov, P.V., Potemkin, D.I., Rebrov, E.V., Sobyanin, V.A., Hessel, V., and Schouten, J.C., *Chem. Eng. J.*, 2010, vol. 160, p. 923.
24. Snytnikov, P.V., Popova, M.M., Men, Y., Rebrov, E.V., Kolb, G., Hessel, V., Schouten, J.C., and Sobyanin, V.A., *Appl. Catal., A*, 2008, vol. 350, p. 53.
25. Ouyang, X. and Besser, R.S., *J. Power Sources*, 2005, vol. 141, p. 39.
26. Ouyang, X., Bednarova, L., Besser, R.S., and Ho, P., *AIChE J.*, 2005, vol. 51, p. 1758.
27. Kolb, G., Schürer, J., Tiemann, D., Wichert, M., Zapf, R., Hessel, V., and Löwe, H., *J. Power Sources*, 2007, vol. 171, p. 198.
28. Delsman, E.R., Laarhoven, B.J.P.F., de Croon, M.H.J.M., Kramer, G.J., and Schouten, J.C., *Chem. Eng. Res. Des.*, 2005, vol. 83, p. 1063.
29. Potemkin, D.I., Snytnikov, P.V., Rebrov, E.V., Hessel, V., and Sobyanin, V.A., *VIII Int. Conf. on Mechanisms of Catalytic Reactions*, Novosibirsk, 2009, vol. 1, p. 83.
30. Snytnikov, P.V., Potemkin, D.I., Rebrov, E.V., Hessel, V., and Sobyanin, V.A., *EuropaCat IX*, Salamanca, Spain, 2009, p. 462.
31. Armatas, G.S., *Chem. Eng. Sci.*, 2006, vol. 61, p. 4662.
32. *Kratkii spravochnik fiziko-khimicheskikh velichin* (Concise Handbook of Physicochemical Data), St. Petersburg: Spetsial'naya Literatura, 1999, p. 203.
33. Satterfield, Ch., *Heterogeneous Catalysis in Practice*, New York: McGraw-Hill, 1980.